Journal of Power Sources 219 (2012) 29–35

Contents lists available at SciVerse ScienceDirect

Journal of Power Sources

journal homepage: www.elsevier.com/locate/jpowsour

Conversion of diatomite to porous Si/C composites as promising anode materials for lithium-ion batteries

Ming-Shan Wang [a], Li-Zhen Fan [a,*], Mian Huang [b], Jinhong Li [c], Xuanhui Qu [a]

[a] School of Materials Science and Engineering, University of Science and Technology Beijing, Beijing 100083, China
[b] Department of Materials Science and Engineering, and State Key Lab of New Ceramics and Fine Processing, Tsinghua University, Beijing 100084, China
[c] Beijing Key Laboratory of Water Resource and Engineering, School of Materials Science and Technology, China University of Geosciences, Beijing 100083, China

HIGHLIGHTS

► Diatomite was used as a raw material for the preparation of porous Si/C composite.
► The pore structure of diatomite could be well retained in the prepared porous Si.
► The porous Si/C composite exhibits high electrochemical performance.

ARTICLE INFO

Article history:
Received 18 April 2012
Received in revised form
27 June 2012
Accepted 30 June 2012
Available online 25 July 2012

Keywords:
Lithium-ion batteries
Anode materials
Silicon
Porous carbon
Composites

ABSTRACT

Diatomite, a natural clay mineral, is mainly composed of silica and contains a large number of fine microscopic pores. In the present work, a series of porous Si/C composites are successfully synthesized by employing diatomite as a raw material, followed by low temperature magnesiothermic reduction, impregnation and carbonization of phenolic resin. The obtained Si/C composites are consisted of porous Si coated with a 15 nm thick amorphous layer of carbon. Porous Si/C composites with different ratios of Si and C are investigated as anode materials for Li-ion batteries. The porous Si/C composite containing 33% carbon exhibits the highest reversible capacity of about 1628 mAh g^{-1} at the first cycle with excellent capacity retention in the following cycles. Moreover, the porous Si/C composites display the excellent rate performance at high current densities such as 1 and 2 A g^{-1}. The optimum electrochemical performance could also be tuned by varying the proportions of porous Si and carbon precursors during the preparation process. The results indicate that the natural pore structures of Si and C are conducive to the electrochemical performance and clay mineral diatomite could be considered as a promising raw material for Si/C composites for lithium-ion batteries.

1. Introduction

The development of safe, low cost, high energy density and long lasting rechargeable lithium-ion batteries greatly depends on the research and application of lithium storage materials. During the past, graphite has been considered as potential candidate for the anode material in lithium-ion batteries due to its excellent cycling performance as well as safe nature [1]. However, the theoretical capacity of graphite is only 372 mAh g^{-1}, which is far below in meeting the demands of high performance lithium-ion batteries. It is of utmost importance to develop new electrode materials exhibiting higher power as well as energy densities [2]. Si is one of the attractive anode materials for lithium-ion batteries because of its highest capacity of 4200 mAh g^{-1} among all the anode materials [3]. Nevertheless, the practical utilization of Si as anode material is hindered by its huge volume changes induced by the lithium-ion insertion and extraction processes, culminating in the pulverization of electrode structure as well as the poor cycling performance [4]. During the recent years, various approaches have been employed to overcome the limitations such as rapid loss of capacity and poor cycling performance. One approach involves the synthesis of novel nanostructured Si such as Si nanospheres [5–7], porous Si [8–10], and Si nanowires [11–13]. The other way is to disperse Si in metallic compounds [14–16] or carbon matrix [10,17–22]. Of all the approaches employed previously, the dispersion of Si into carbon matrix has attracted particular interest owing to the fact that carbonaceous materials can accommodate the volume expansion of Si during its alloying/de-alloying processes, and moreover, also maintain good electronic conductivity during charging/discharging cycles.

* Corresponding author. Tel./fax: +86 10 62334311.
E-mail address: fanlizhen@ustb.edu.cn (L.-Z. Fan).

0378-7753/$ – see front matter © 2012 Elsevier B.V. All rights reserved.
http://dx.doi.org/10.1016/j.jpowsour.2012.06.102

Uptill now, various methods have been adopted to fabricate porous, hollow or one-dimensional nanostructured Si-based electrode materials. These methods include chemical reduction [23,24], thermal decomposition [25,26], and chemical vapor deposition [13,27,28]. The siliceous precursors used are mainly comprised of Si-containing polymers [13,29–31], silicohydride [26,32], and silica [24,33]. However, the strategies, mentioned above, possess the disadvantages such as rigorous experimental conditions, complicated processing, and expensive raw materials. For instance, in order to synthesize one-dimensional Si nanowires, Au is generally utilized as catalyst in combination with high pressure and high temperature conditions. On the other hand, the preparation of three-dimensional porous Si involves the utilization of SBA-15 or triethanolamine as template. The time-consuming removal of template along with the use of dangerous corrosive agent such as HF limits the application of this process.

Diatomite is a natural biological sedimentary mineral obtained from the accumulation and deposition of unicellular aquatic plankton [34]. It is mainly comprised of SiO_2 with small concentrations of Fe_2O_3, Al_2O_3, MgO, CaO, and organic matters. It is widely used as heat insulation, filter, and absorbent material because of its numerous fine microscopic pores, large specific surface area, and high absorption capacity [35]. Herein, we report the utilization of the diatomite as a raw material for the fabrication of porous Si/C composites. We have employed a facile, low cost, and green strategy to fabricate these composites. In contrast to the template method involving complicated processes, our process has demonstrated improved performance and efficiency. Firstly, the fine numerous natural pores of diatomite also remain intact following the purification and low temperature treatment. Secondly, the fabrication process from diatomite to porous Si is environmentally friendly, low cost, and simple, which can be used for large scale production. Moreover, the pulverization of the electrode can be suppressed effectively by using the Si/C composite, and more importantly, the excellent cyclability and rate capability are acquired with these composites.

2. Experimental

2.1. Materials

Diatomite (Shuangjiang, Yunnan province, China) was purified by the following process. Mg powder (99.9%, Aldrich) and phenolic resin (99%, Zhenjiang Hengtong Chemical Co. Ltd) were used as received. All solutions were prepared in deionized water. All other chemical reagents were in analytical grade.

2.2. Materials synthesis

2.2.1. Purification of diatomite

Natural diatomite was ground and infiltrated in water with 0.01 M NaOH, and then suspension was collected by filtering and drying. Subsequently, diatomite was calcined at 800 °C for 2 h in air to remove the organic matters and poured into 6 M H_2SO_4 at 95 °C to remove the impurity such as Fe_2O_3, Al_2O_3, MgO, and CaO. Finally, the purified diatomite was filtrated, washed, and then dried.

2.2.2. Conversion of diatomite to porous Si

The purified diatomite was mixed with Mg powder with the mass ratio of 1:1, and calcined at 650 °C under Ar atmosphere for 6 h, and subsequently, the porous Si was obtained by removing the redundant Mg, MgO and Mg_2Si with 0.1 M HCl solution.

2.2.3. Preparation of porous Si/C composites

Porous Si and phenolic resin with weight ratios of 1:1, 1:5, and 1:15 were mixed in acetone. The mixture was carbonized at 750 °C under Ar atmosphere for 2 h at a heating rate of 5 °C min^{-1} to obtain porous Si/C composites. As a comparison, phenolic resin was also carbonized under the same experimental conditions.

2.3. Structural characterization

The thermogravimetric analysis was carried out by using a TGA/DSC1 type instrument (Mettler Toledo, Switzerland) from 20 to 1200 °C with a heating rate of 10 °C min^{-1} in air. The sample hold is alumina crucible with 70 uL volume which was previously stabilized by heating at high temperature. The phase composition of diatomite, porous Si, and porous Si/C composites were determined by X-ray diffraction (XRD) on a Rigaku D/max-RB diffractometer using Cu Kα radiation at 40 kV and 30 mA, with a step of 0.02° between 10 and 90°. Raman spectra were recorded using HR800 (Horiba JobinYvon) with a 514.5 nm Ar-ion laser. Field-Emission Scanning Electron Microscopy (FE-SEM) analysis was conducted with a JEOL JSM-6330 electron microscope. Transmission Electron Microscopy (TEM) and Selected Area Electron Diffraction (SAED) images were recorded by a JEM-2100F transmission electron microscope. The pore structures were measured from a nitrogen adsorption–desorption isotherm at 77 K after being degassed at 300 °C for at least 3 h using a Quantachrome Autosorb-IQ2.

2.4. Electrochemical measurements

The working electrodes were prepared by mixing 40 wt% active materials, 40 wt% acetylene black and 20 wt% polyvinylidene-fluoride dissolved in N-methylpyrrolidinone. The resulting slurry was then spread uniformly on the copper foil and dried at 120 °C in vacuum for 12 h. Electrochemical measurements were performed with two-electrode employing the prepared electrode as the working electrode and lithium foil as the counter electrode. The electrolyte was 1 M $LiPF_6$ in a mixed solvent of ethylene carbonate, diethyl carbonate and ethyl methyl carbonate with volume ratio of 1:1:1. The charge/discharge performance of the electrodes was evaluated at 25 °C using an automatic battery testing system (LAND CT2001A) at a voltage window of 0.01–1.5 V. Electrochemical impedance spectroscopy (EIS) was recorded from 105 to 0.01 Hz by

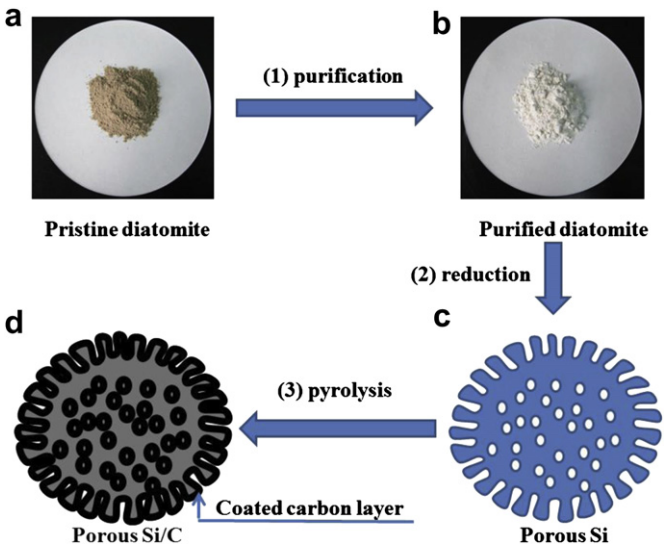

Fig. 1. The schematic fabrication of porous Si/C composite: (1) purification of diatomite by calcination and acid treatment; (2) preparation of the porous Si electrode by reduction with Mg; (3) preparation of porous Si/C composites by the pyrolysis of phenolic resin.

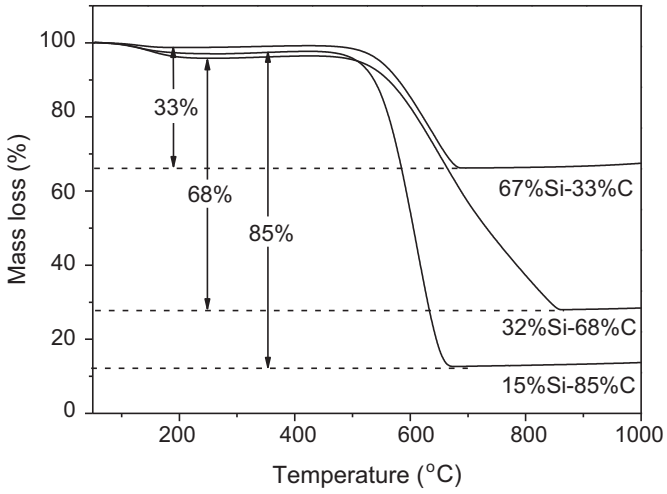

Fig. 2. Thermogravimetric analysis curves of porous Si/C composites with different weight ratios of porous Si and phenolic resin.

using an electrochemical workstation (CHI660C) and the amplitude of the used perturbation was 10 mV. The cells were measured before cycle and after 5 cycles. The open circuit voltage (OCV) of the cells before cycle was maintained at 2.7 V. After 5 cycles, the cells were maintained at charged state (Li extraction) while the OCV are at 0.5 V. The specific capacity of composites was calculated according to the weight of active materials.

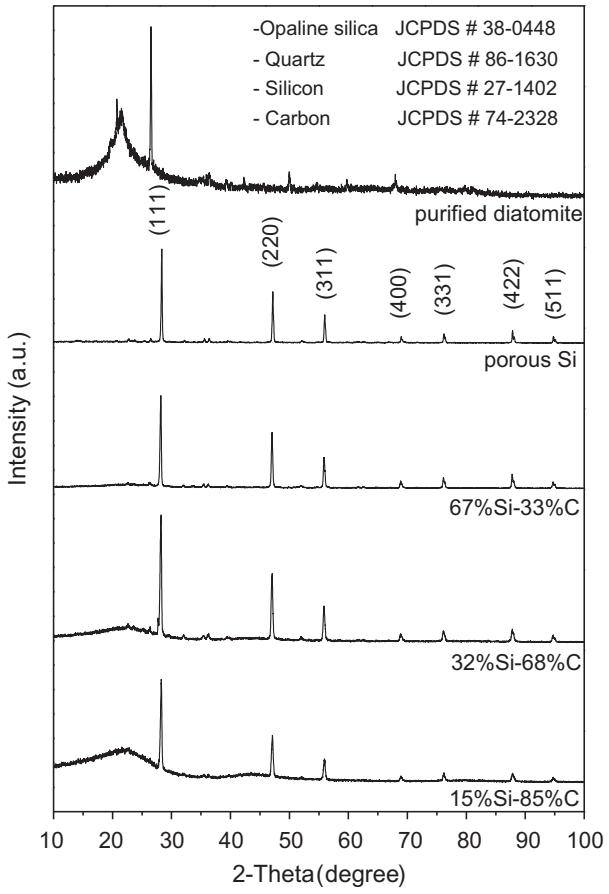

Fig. 3. XRD patterns of purified diatomite, porous Si, and porous Si/C composites with different ratios of porous Si and C.

3. Results and discussion

The schematic fabrication of porous Si/C composite is illustrated in Fig. 1. Firstly, diatomite is calcined and treated with acid to remove the organic matters and other oxides. The color of the diatomite becomes white following removal of impurity. Subsequently, diatomite reacts with Mg under Ar atmosphere to form the porous Si in accordance with the following reaction:

$$2Mg(g) + SiO_2(s) \rightarrow 2MgO(s) + Si(s)$$

During the process, the excessive Mg could also react with Si as the following reaction:

$$Mg(g) + Si(s) \rightarrow Mg_2Si(s)$$

After the reduction reaction, the excess Mg, MgO and Mg_2Si can be easily removed with HCl washing. Then the purified porous Si is mixed with carbon precursor phenolic resin and further pyrolyzed under Ar atmosphere, resulting in the porous Si/C composites. The carbon contents in the porous Si/C composites, determined by thermogravimetric analysis (Fig. 2), are found to be 33 wt%, 68 wt%, and 85 wt% for porous Si:phenolic resin = 1:1, 1:5, 1:15, respectively. The corresponding porous Si/C composites are termed as 67% Si–33%C, 32%Si–68%C, and 15%Si–85%C, respectively.

The XRD patterns of purified diatomite, porous Si, and porous Si/C composites are shown in Fig. 3. The phase composition of the purified diatomite is mostly comprised of hydrous silica as opaline silica along with the small amount of other crystalline phase identified as quartz. Following the magnesiothermic reduction, porous Si exhibits the high crystallinity. The peaks of Mg, MgO and

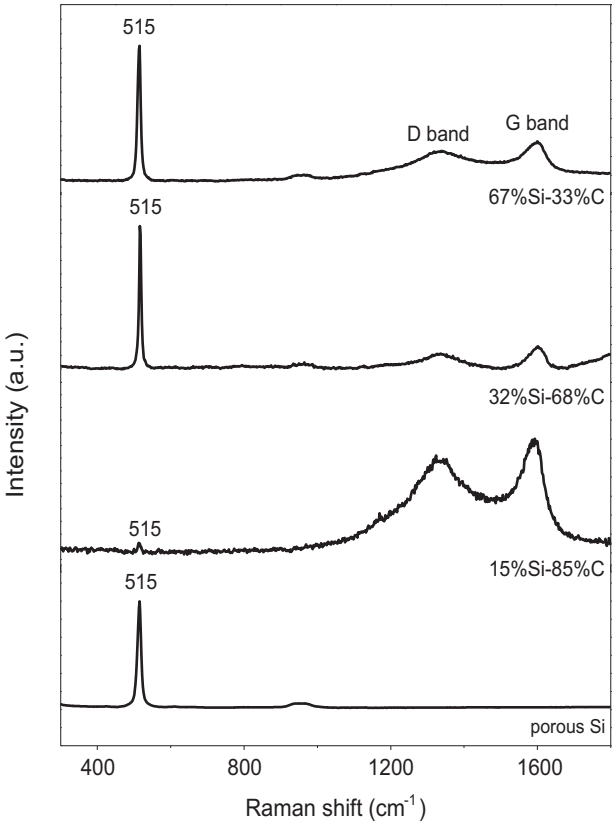

Fig. 4. Raman spectra of porous Si and porous Si/C composites with different ratios of porous Si and C.

Mg_2Si cannot be detected. The XRD patterns of porous Si/C composites indicate that the crystal structure of Si remains intact during the pyrolysis process. In addition, the diffraction peaks corresponding to the graphite have not been detected in the XRD pattern, which is possibly due to the formation of the amorphous structure of carbon at low temperature [36].

The Raman spectra of porous Si/C composites, containing different ratios of porous Si and carbon, are exhibited in Fig. 4. The band at 515 cm^{-1} corresponds to the crystalline Si [37]. After the carbon coating, the characteristic peaks around 1335 cm^{-1} (the "D band") and 1594 cm^{-1} (the "G band") appear for different ratios of porous Si and carbon, which are the typical peaks assigned to the disorder in the graphene layers of carbon materials and the in-plane phonon modes of graphene, respectively [21,38]. The ratios of intensity between D and G band are 0.88, 0.85, and 0.84 for 67% Si–33%C, 32%Si–68%C, and 15%Si–85%C, respectively, indicating the low degree graphitization of composites. Furthermore, the relative intensity between carbon and Si has notably changed. This phenomenon may be explained by two factors. Firstly, the increase of the phenolic resin contents renders more carbon coating at the surface of porous Si. Secondly, the scattering intensity at the surface of carbon is stronger than that of Si.

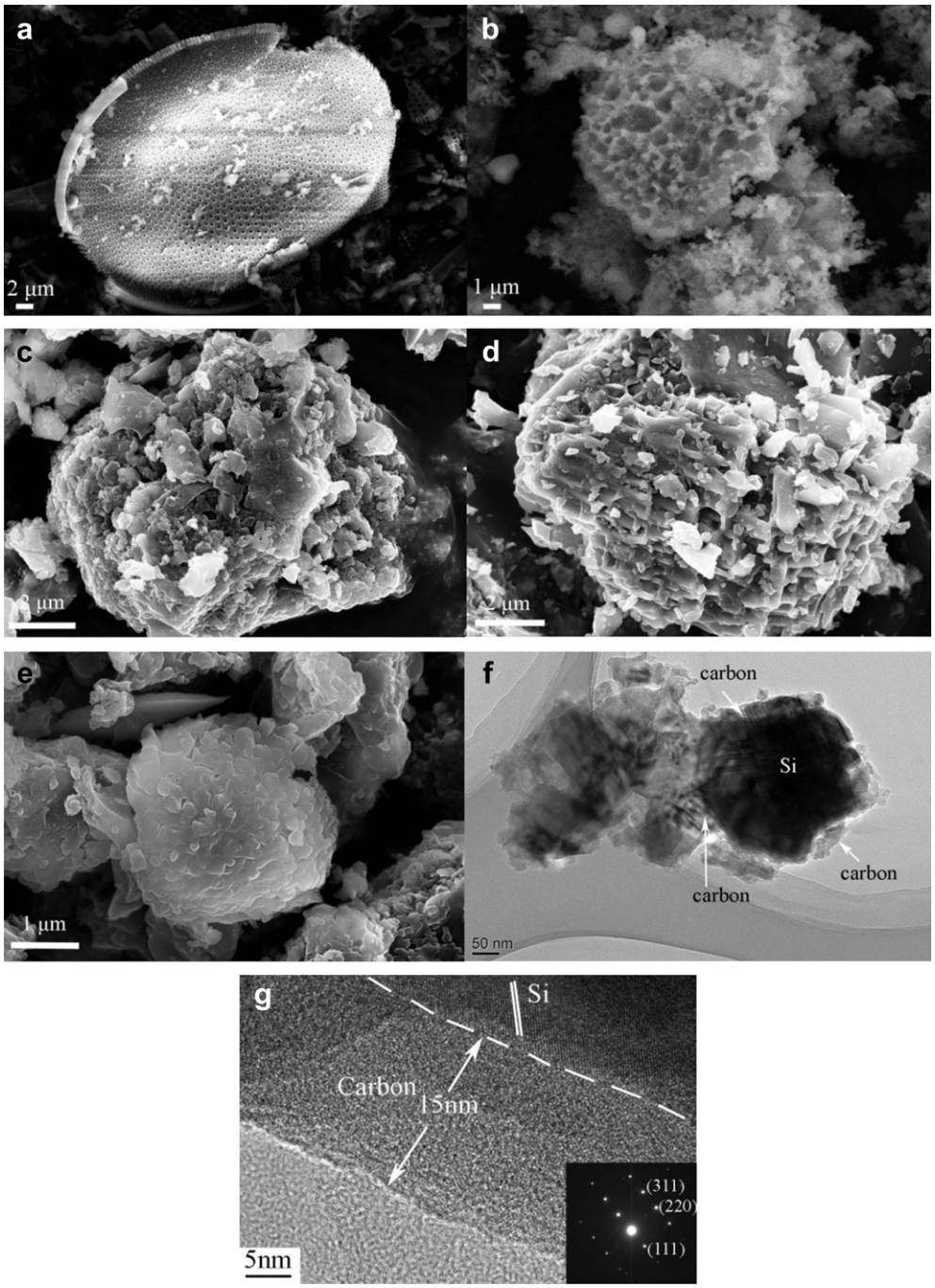

Fig. 5. FE-SEM of (a) purified diatomite, (b) porous Si, (c) 67%Si–33%C, (d) 32%Si–68%C, (e) 15%Si–85%C, HR-TEM of (f) and (g) 67%Si–33%C and the inset (g) shows SAED for porous Si.

Fig. 5a reveals the FE-SEM image of the primitive diatomite. It is composed mainly of fine microscopic pores, cavities, and channels. It is evident in Fig. 5b that after reacting with Mg (Fig. 5b), a large concentration of three-dimensional (3D) pores and channels still exists above as well as inside the porous Si particles. It is believed that the porous structure is beneficial to overcome the problem associated with the volume change of Si induced by the Li-ion insertion/extraction [8]. It is obvious in Fig. 5c and d that with the carbon contents of 33% and 67%, the carbon has not only filled within the channels of porous Si, but the surface of porous Si has also been coated by the carbon. Meanwhile, the rough surface of porous Si is still maintained. When the carbon content increases to 85% (Fig. 5e), the porous Si is completely covered by carbon layer. Surface of the particle is much smooth than that of 67%Si–33%C and 32%Si–68%C. To further identify the carbon distribution within the interior of micro-sized particles, TEM analysis is performed. As shown in Fig. 5f, the carbon not only coated on the surface of porous Si, but also existed in the channels (arrow in the figure). A relatively disordered microstructure in Fig. 5g clearly reveals that the surface of particles exhibits a uniform layer of the carbon coating with the thickness of about *ca.* 15 nm. It is also noted in SAED micrographs (inset in Fig. 5g) that the porous Si, formed by magnesiothermic reduction, depicts a spot pattern of Si (011), $(11\bar{1})$, and (200), corroborating the existence of single crystalline Si.

The nitrogen adsorption–desorption isotherms measurements are further performed to comprehend the formation mechanism of porous Si and Si/C composites derived from the porous diatomite. It is evident in Fig. 6 that the nitrogen adsorption–desorption isotherms, for purified diatomite and porous Si, are characteristic of type IV, indicating the presence of both micropores and mesopores. However, as the relative pressure $P/P_0 > 0.45$, the purified diatomite and porous Si exhibit a H1 hysteresis loop, which is the characteristic of aggregates of particles forming channel-like pores. Furthermore, the calculated specific surface areas, listed in Table 1, indicate that the total, mesopore, and macropore surface areas of the porous Si decrease, but the micropore surface area increases. It implies that the porous Si still retains a large concentration of mesopores and macropores and more micropores appear after magnesiothermic reduction. After the carbon coating, the nitrogen adsorption–desorption isotherms of the porous Si/C composites are classified as type I, suggesting the presence of micropores. The total surface area, total pore volume, and the micropore volume of porous Si/C increase with increasing carbon contents, testifying that a large amount of microporous carbon has formed during the pyrolysis of phenolic resin. The high specific area and pore volume of porous Si/C are conducive to the permeation of the electrolyte and the transfer of Li-ion.

The porous Si and porous Si/C (with different ratios of porous Si and carbon) are tested as anode materials for Li-ion batteries. Fig. 7a displays the discharge (lithium alloying) and charge (lithium de-alloying) curves of porous Si and porous Si/C composites during the first cycle in the voltage window of 0.01–1.5 V and at the current density of 50 mA g^{-1}. The first cycle discharging of porous Si exhibits a flat and smooth voltage plateau at 0.11 V and charging voltage plateau at 0.45 V, which is similar to the behavior of crystalline Si [39]. The first charging and discharging specific capacities of porous Si are 1826 and 2666 mAh g^{-1}, respectively, with a coulombic efficiency of 68.5%. The relatively large initial irreversible capacity may be ascribed to the following reasons: Firstly, the alloying of Si with lithium results in a partly irreversible phase transformation of silicon during the first charge/discharge cycle [40,41]; Secondly, the direct contact between Si and electrolyte results in the electrochemical reduction of the electrolyte and the formation of solid electrolyte interphase (SEI) film inside the pores and at the surface of Si particles. The formation of SEI implies the consumption of some active lithium [42]. After 30 cycles, the charge capacity of porous Si is only 240 mAh g^{-1} (Fig. 7b), which indicates a large capacity loss. The rapid capacity loss is rendered by the pulverization of the electrode materials during lithium insertion/extraction processes and also the ongoing formation of SEI film on the surface of particles. For a comparison purpose, the charge capacity of bare carbon is found to be at 400 mAh g^{-1}. Apparently,

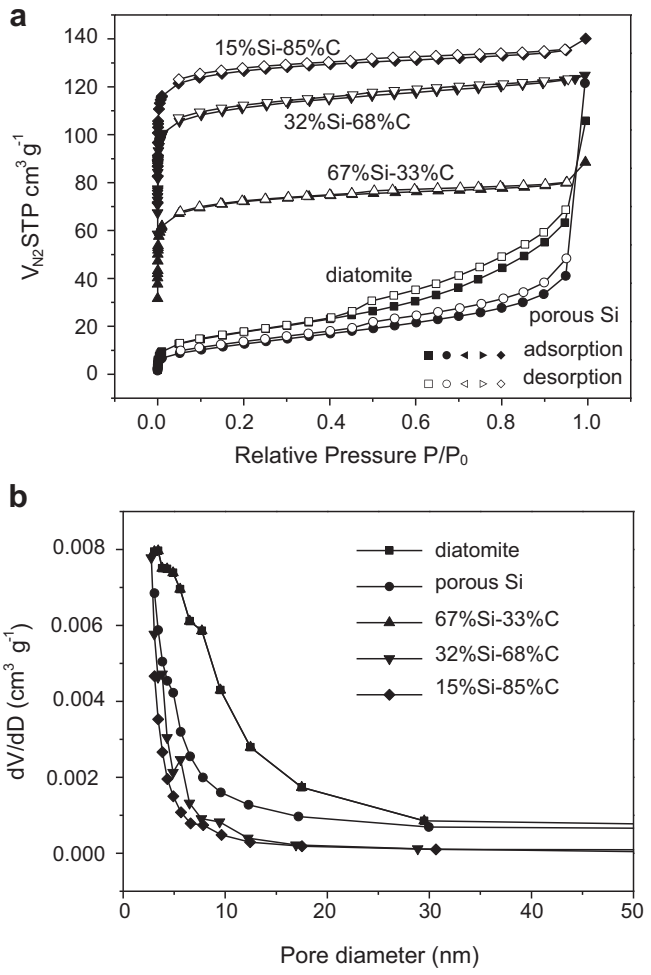

Fig. 6. (a) Nitrogen adsorption–desorption isotherms and (b) pore size distribution of purified diatomite, porous Si, and porous Si/C composites with different ratios of porous Si and C.

Table 1
Surface area and porosity of purified diatomite, porous Si, and porous Si/C composite.

Sample	S_{total} (m^2 g^{-1})[a]	S_{micro} (m^2 g^{-1})[b]	$S_{meso+macro}$ (m^2 g^{-1})[c]	V_{total} (cm^3 g^{-1})[d]	V_{micro} (cm^3 g^{-1})[e]	APD (nm)[f]
Diatomite	63.4	0	63.4	0.164	0	3.42
Porous Si	46.9	6.0	40.9	0.188	0.003	3.07
67%Si–33%C	274.3	260.1	14.1	0.137	0.108	3.07
32%Si–68%C	438.0	407.8	30.2	0.193	0.161	1.43
15%Si–85%C	504.2	488.1	16.1	0.217	0.191	3.07

[a] Total surface areas (S_{total}) are derived using the multipoint Brauner–Emmett–Teller (BET) method.
[b] Micropore areas (S_{micro}) are calculated from the *t*-plot.
[c] Mesopore and macropore areas ($S_{meso+macro}$) are calculated by subtracting S_{micro} from S_{total}.
[d] Total pore volume (V_{total}) at $P/P_0 = 0.99$.
[e] V_{micro}: Micropore volume.
[f] APD: Average pore diameter are calculated by using BJH model.

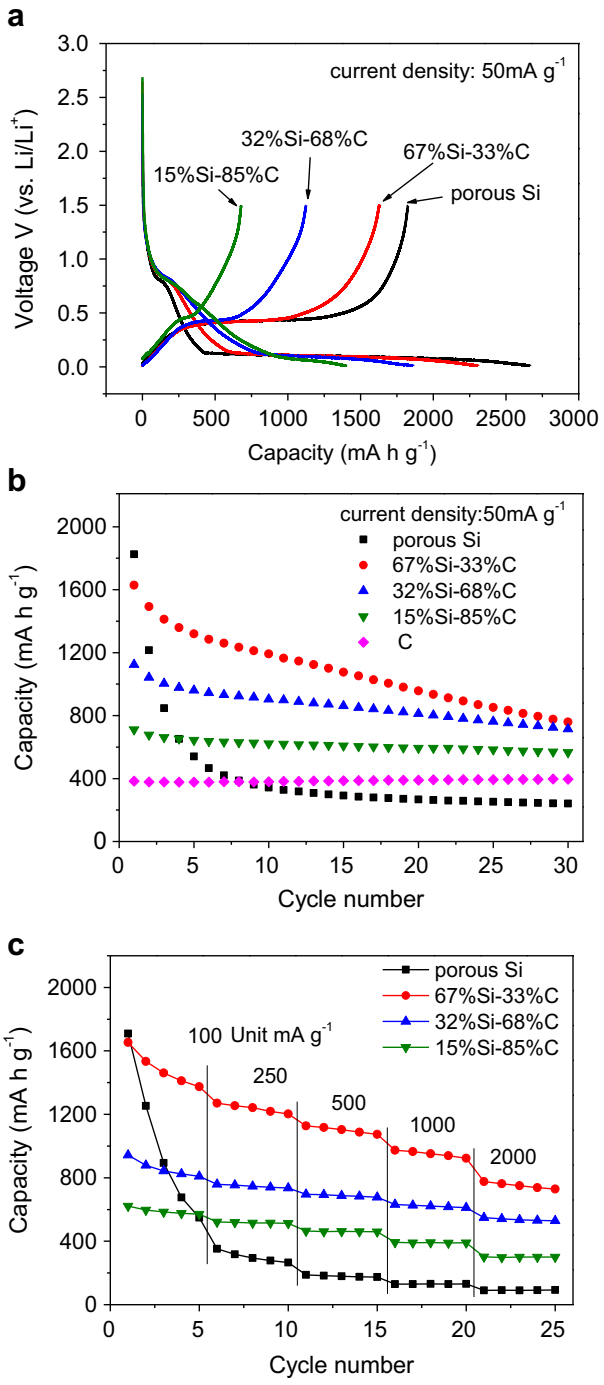

Fig. 7. Electrochemical performance of porous Si and porous Si/C composites with different ratios of porous Si and C: (a) the first charge–discharge curves at 50 mA g^{-1} between voltage limits of 0.01–1.5 V, (b) cycling performance at a current density of 50 mA g^{-1}, and (c) rate stabilities at various current densities.

after carbon coating, the main charge and discharge voltage plateaus of porous Si/C composites are similar to that of porous Si, indicating that the porous Si contributes to most of the overall anode capacity. The initial charge capacities of 67%Si–33%C, 32% Si–68%C, and 15%Si–85%C are 1628, 1125, and 711 mAh g^{-1}, respectively, while the initial coulombic efficiencies of three compositions are 70.5%, 60.4%, and 50.7%, respectively. The enhancement in the initial irreversible capacity of composites with increasing carbon contents can be ascribed to the increased specific surface area of composites (Table 1). The more contact between the composites and electrolyte facilitates the formation of SEI film. The porous Si/C composites present the higher capacity retention compared to that of the pure porous Si (Fig. 7b). The higher reversible charge capacity of 759, 715, and 567 mAh g^{-1} for 67% Si–33%C, 32%Si–68%C, and 15%Si–85%C, respectively, is acquired after 30 cycles. The coulombic efficiencies of 67%Si–33%C, 32% Si–68%C, and 15%Si–85%C rise to 93%, 96% and 97% after 10 cycles. The increased specific capacity and cycling performance of the porous Si/C composites can be attributed to the existence of micropores in the composites which can buffer the expansion of porous Si during the Li-ion insertion/extraction. Another reason for the amelioration of specific capacity and cycling performance can be assigned to the presence of carbon, which can provide more pathways for the electron transportation and ultimately suppress the polarization. Hence, by increasing the carbon contents, the better cycling properties of porous Si/C composites can be obtained albeit the capacity is slightly decreased. As the carbon contents are further increased to 68%, the 32%Si–68%C composite displays excellent cycle performance and high capacity retention. Nonetheless, the continuous increase of carbon contents will ultimately deteriorate the capacity of composite owing to the fact that the specific capacity of carbon is much lower than that of Si.

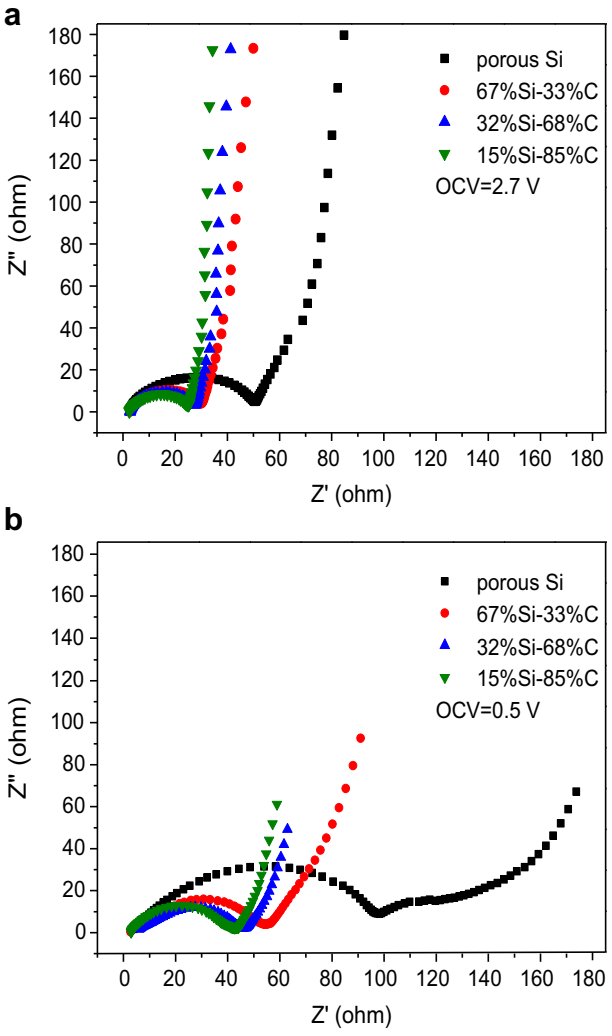

Fig. 8. Nyquist plots of the electrodes for porous Si and porous Si/C composites with different ratios of porous Si and C: (a) before cycling and (b) after 5 cycles (in the de-lithiated state).

In order to further investigate the electrochemical performance of porous Si/C composites, the rate capabilities of porous Si and Si/C composites are compared and results are presented in Fig. 7c. In the case of relatively low charge/discharge rate (100 mA g^{-1}), the initial charged capacities of 67%Si–33%C, 32%Si–68%C, and 15%Si–85%C are1653, 943, and 621 mAh g^{-1}, respectively. Increasing the current density to 2000 mA g^{-1}, the reversible capacities of 67% Si–33%C, 32%Si–68%C, and 15%Si–85%C reach up to 776, 549, and 302 mAh g^{-1}, respectively albeit the capacity of porous Si is only found to be 90 mAh g^{-1}. The excellent rate capabilities may be attributed to the uniform carbon layer, which improves the electrical conductivity of the composite and accelerates the transport of lithium-ion.

In order to discern the mechanism of the capacity degradation of porous Si and porous Si/C composites, EIS measurements are carried out and the resulting Nyquist plots of porous Si and porous Si/C composites are compared before and after the 5 cycles. The typical impedance plots (Z′ vs. Z″) for porous Si and porous Si/C are displayed in Fig. 8a, demonstrating a normal impedance behavior such as a depressed semicircular portion followed by linear portion with angle considerably more than 45°. After 5 cycles, the diameters of the semicircles of porous Si and porous Si/C composites become larger than that before cycling (Fig. 8b), and an additional semicircle appears for porous Si. The semicircles, presented at high and medium frequency region, correspond to the interface resistance of porous Si and porous Si/C, which is associated with the SEI film and charge-transfer resistance of Li-ion insertion. The linear portions of low frequency region correspond to the diffusion of Li-ion in the composites [43,44]. It can be noticed that the resistance of SEI film of porous Si is much larger than that of the porous Si/C composites after cycling, indicating that the thicker SEI film is formed at the surface of porous Si. Moreover, the resistance of charge transfer in porous Si is larger than that in porous Si/C composites, facilitating the faster diffusion and transportation of Li-ion n the porous Si/C composites than that in porous Si.

4. Conclusions

Diatomite, a natural clay mineral with abundant pore structures, has been employed, for the first time, as a raw material for the preparation of porous Si/C composite utilized as anode material for lithium-ion batteries. Firstly, diatomite has been converted into porous Si by a simple low temperature heat treatment without losing its fine natural pore structure. The porous Si/C composites are synthesized by dispersing porous Si into carbon precursor and a subsequent pyrolysis process. The porous Si/C composites prepared by diatomite have exhibited high specific surface areas with large concentration of pores, facilitating the diffusion of Li-ion and the penetration of electrolyte by providing more favorable paths. The effectiveness of the porous structure and the higher carbon contents in buffering the volume expansion, preserving the integrity of Si particles, and serving as a good conductor matrix accounts for the excellent electrochemical performance of the composites for the rechargeable lithium-ion batteries. The results of present investigation demonstrate the potential feasibility of fabricating porous Si/C composites by natural clay mineral diatomite. The present work has proposed an environmental friendly and price competitive approach for the production of Si/C anode materials.

Acknowledgments

This work was supported by NSF of China and Fundamental Research Funds for the Central Universities of China.

References

[1] J. Dahn, T. Zheng, Y. Liu, J. Xue, Science 270 (1995) 590–593.
[2] V. Etacheri, R. Marom, R. Elazari, G. Salitra, D. Aurbach, Energy Environ. Sci. 4 (2011) 3243–3262.
[3] P. Poizot, S. Laruelle, S. Grugeon, L. Dupont, J. Tarascon, J. Power Sources 97 (2001) 235–239.
[4] R.A. Huggins, J. Power Sources 81 (1999) 13–19.
[5] H. Li, X. Huang, L. Chen, Z. Wu, Y. Liang, Electrochem. Solid-State Lett. 2 (1999) 547–549.
[6] M. Holzapfel, H. Buqa, L.J. Hardwick, M. Hahn, A. Würsig, W. Scheifele, P. Novák, R. Kötz, C. Veit, F.M. Petrat, Electrochim. Acta 52 (2006) 973–978.
[7] J.R. Szczech, S. Jin, Energy Environ. Sci. 4 (2011) 56–72.
[8] H. Kim, J. Cho, Nano Lett. 8 (2008) 3688–3691.
[9] Y. Zheng, J. Yang, J. Wang, Y. NuLi, Electrochim. Acta 52 (2007) 5863–5867.
[10] C. Du, M. Chen, L. Wang, G. Yin, J. Mater. Chem. 21 (2011) 15692–15697.
[11] B.M. Bang, H. Kim, J.P. Lee, J. Cho, S. Park, Energy Environ. Sci. 4 (2011) 3395–3399.
[12] Y. Qu, H. Zhou, X. Duan, Nanoscale 3 (2011) 4060–4068.
[13] C.K. Chan, R.N. Patel, M.J. O'Connell, B.A. Korgel, Y. Cui, Nano Lett. 4 (2010) 1443–1450.
[14] P. Patel, I.S. Kim, P. Kumta, Mater. Sci. Eng. B 116 (2005) 347–352.
[15] Z. Zeng, J. Tu, Y. Yang, J. Xiang, X. Huang, F. Mao, M. Ma, Electrochim. Acta 53 (2008) 2724–2728.
[16] Y. Liu, B. Chen, F. Cao, H.L.W. Chan, X. Zhao, J. Yuan, J. Mater. Chem. (2011) 17083–17086.
[17] W. Wang, P.N. Kumta, Nano Lett. 4 (2010) 2233–2241.
[18] J. Yang, B. Wang, K. Wang, Y. Liu, J. Xie, Z. Wen, Electrochem. Solid-State Lett. 6 (2003) A154–A156.
[19] P. Gao, J. Fu, J. Yang, R. Lv, J. Wang, Y. Nuli, X. Tang, Phys. Chem. Chem. Phys. 11 (2009) 11101–11105.
[20] Y. Xu, G. Yin, Y. Ma, P. Zuo, X. Cheng, J. Mater. Chem. 20 (2010) 3216–3220.
[21] J. Guo, X. Chen, C. Wang, J. Mater. Chem. 20 (2010) 5035–5040.
[22] G. Wang, J. Ahn, J. Yao, S. Bewlay, H. Liu, Electrochem. Commun. 6 (2004) 689–692.
[23] H. Kim, B. Han, J. Choo, J. Cho, Angew. Chem. Int. Ed. 120 (2008) 10305–10308.
[24] Y. Yao, M.T. McDowell, I. Ryu, H. Wu, N. Liu, L. Hu, W.D. Nix, Y. Cui, Nano Lett. 11 (2011) 2949–2954.
[25] P. Shen, N. Uesawa, S. Inasawa, Y. Yamaguchi, J. Mater. Chem. 20 (2010) 1669–1675.
[26] Y. Kumai, H. Kadoura, E. Sudo, M. Iwaki, H. Okamoto, Y. Sugiyama, H. Nakano, J. Mater. Chem. 21 (2011) 11941–11946.
[27] T. Song, J. Xia, J.H. Lee, D.H. Lee, M.S. Kwon, J.M. Choi, J. Wu, S.K. Doo, H. Chang, W.I. Park, Nano Lett. 10 (2010) 1710–1716.
[28] H. Wolf, Z. Pajkic, T. Gerdes, M. Willert Porada, J. Power Sources 190 (2009) 157–161.
[29] L.F. Cui, R. Ruffo, C.K. Chan, H. Peng, Y. Cui, Nano Lett. 9 (2009) 491–495.
[30] B. Fuchsbichler, C. Stangl, H. Kren, F. Uhlig, S. Koller, J. Power Sources 196 (2011) 2889–2892.
[31] J.K. Lee, M.C. Kung, L. Trahey, M.N. Missaghi, H.H. Kung, Chem. Mater. 21 (2008) 6–8.
[32] M. Holzapfel, H. Buqa, W. Scheifele, P. Novák, F.M. Petrat, Chem. Commun. (2005) 1566–1568.
[33] Y. Yu, L. Gu, C. Zhu, S. Tsukimoto, P.A. van Aken, J. Maier, Adv. Mater. 22 (2010) 2247–2250.
[34] J. Stosur, A. David, J. Pet. Technol. 28 (1976) 1138–1144.
[35] H. Hadjar, B. Hamdi, M. Jaber, J. Brendlé, Z. Kessaïssia, H. Balard, J. Donnet, Micropor. Mesopor. Mat. 107 (2008) 219–226.
[36] P. Zuo, G. Yin, Y. Ma, Electrochim. Acta 52 (2007) 4878–4883.
[37] R. Tsu, H. Shen, M. Dutta, Appl. Phys. Lett. 60 (1992) 112–114.
[38] J.T. McCann, B. Lim, R. Ostermann, M. Rycenga, M. Marquez, Y. Xia, Nano Lett. 7 (2007) 2470–2474.
[39] M. Obrovac, L. Krause, J. Electrochem. Soc. 154 (2007) A103–A108.
[40] M.N. Obrovac, L. Christensen, Electrochem. Solid-State Lett. 7 (2004) A93–A96.
[41] J.H. Ryu, J.W. Kim, Y.-E. Sung, S.M. Oh, Electrochem. Solid-State Lett. 7 (2004) A306–A309.
[42] X. Wu, Z. Wang, L. Chen, X. Huang, Electrochem. Commun. 5 (2003) 935–939.
[43] A. Funabiki, M. Inaba, Z. Ogumi, S. Yuasa, J. Otsuji, A. Tasaka, J. Electrochem. Soc. 145 (1998) 172–178.
[44] Y.C. Chang, H.J. Sohn, J. Electrochem. Soc. 147 (2000) 50–58.